VALIDATION AND VERIFICATION OF STEADY RESISTANCE KCS SIMULATIONS WITH SINKAGE AND TRIM USING EMBEDDED FREE SURFACE METHOD

Inno Gatin (Faculty of Mechanical Engineering and Naval Architecture, Croatia)
Hrvoje Jasak (Faculty of Mechanical Engineering and Naval Architecture, Croatia)
Vuko Vukčević (Faculty of Mechanical Engineering and Naval Architecture, Croatia)

1 SUMMARY

This paper presents detailed validation and verification study for the KCS in calm water conditions. Validation is performed by comparing the resistance, sinkage and trim with experimental data for six Froude numbers, while verification is performed for each case by assessing grid and iterative uncertainties. A single set of governing equations for water and air is used where jump conditions at the free surface are used to discretise discontinuous density and dynamic pressure fields. Volume of Fluid (VOF) method is used for interface capturing, and the k–ω SST model is used for turbulence modelling. Ship motion is solved with quaternion based six degrees–of–freedom (6 DOF) rigid body motion equations. The method is implemented in the Naval Hydro pack based on foam–extend, a community driven fork of OpenFOAM software.

2 INTRODUCTION

Accurate and efficient assessment of the resistance of a ship in calm water is one of the fundamental problems in naval hydrodynamics, traditionally dictated by industrial needs. Most present day CFD algorithms are well established and thoroughly validated for such applications [5]. On the other side, verification studies are equally important in order to assess uncertainties associated with complex CFD algorithms. Only with detailed validation and verification, a CFD algorithm is considered reliable and can used reliably in a design process.
This paper briefly outlines a mathematical and numerical model based on embedding technique, while the emphasis is given to detailed validation and verification studies.

3 MATHEMATICAL MODEL

In this section mathematical model of incompressible two-phase free surface flow is presented. Two–phase model is based on a single set of mixture equations taking into account jump conditions at the free surface implicitly [2]. This embedded free surface approach correctly models density and dynamic pressure discontinuities and thus resolves the problem of parasitic air velocities. The volumetric continuity equation for continuous velocity field $\mathbf{u}$ reads:

$$\nabla \bullet \mathbf{u} = 0. \tag{1}$$

Phase momentum equation for an individual phase, assuming constant density and presence of a sharp free surface reads:

$$\frac{\partial \mathbf{u}}{\partial t} + \nabla \bullet ((\mathbf{u} - \mathbf{u}_M)\,\mathbf{u}) - \nabla \bullet (\nu_e \nabla \mathbf{u}) = -\frac{1}{\rho}\nabla p_d\,, \tag{2}$$

where ρ is the two–phase discontinuous density field, p_d is the dynamic pressure, and ν_e stands for effective kinematic viscosity, allowing for general turbulence modelling [11]. $\mathbf{u}_M$ is the relative grid motion velocity accounting for the moving grid according to the Space Conservation Law [1].
In the present embedded free surface approach, density discontinuity is taken into account exactly, yielding first jump condition:

$$p_d^- - p_d^+ = -(\rho^- + \rho^+)\mathbf{g}\bullet\mathbf{x}\,, \tag{3}$$

where p_d^- and p_d^+ denote dynamic pressure infinitesimally close to the free surface from water and air side, respectively. ρ^- and ρ^+ denote constant densities of water and air. This condition arises from the continuity of the pressure at the free surface: $p^- - p^+ = 0$, which takes the form of equation (3) when the decomposition of the pressure into dynamic and static part is applied: $p = p_d + \rho\mathbf{g}\bullet\mathbf{x}$. In order to facilitate implementation of the second jump condition, tangential stress balance is approximated by usual smearing of the kinematic viscosity across the free surface. Surface tension effects are also neglected. Inspecting the jump of the momentum equation at the free surface [10], a second jump condition arises:

$$\frac{1}{\rho^-}\nabla p_d^- - \frac{1}{\rho^+}\nabla p_d^+ = 0, \quad (4)$$

which balances the density and pressure gradient jump at the free surface. This approach is justified for large scale two–phase problems encountered in naval hydromechanics [2].

Jump conditions (3) and (4) are used to embed the free surface into a single momentum (2) and (1) continuity equation. This is achieved by deriving interface–corrected interpolation schemes for dynamic pressure near the free surface.

VOF transport equation with additional compression term used in this study reads [7]:

$$\frac{\partial \alpha}{\partial t} + \nabla_\bullet((\mathbf{u} - \mathbf{u}_M)\,\alpha) + \nabla_\bullet(\mathbf{u}_r \alpha(1-\alpha)) = 0\,, \quad (5)$$

where α is the volume fraction and $\mathbf{u}_r$ is the compressive velocity field oriented towards the interface in the normal direction. The last convective terms serves to prevent excessive smearing of the interface which only affects the effective viscosity field.

4 NUMERICAL MODEL

Numerical model is based on second–order accurate polyhedral FV method used in foam–extend [4]. Rigid body motion is solved using quaternion based 6 DOF equations. Mesh motion is modelled as a rigid body motion with special boundary conditions. Coupling of pressure, velocity, free surface and 6 DOF equations is performed in a segregated manner using the PIMPLE algorithm.

As the steady state solution is sought, first–order accurate implicit Euler scheme is used for temporal discretisation, while only one motion corrector is used per time–step. Grid motion is under–relaxed with 0.5 in order to damp out oscillatory convergence of sinkage and trim and to achieve the steady state solution faster.

5 VALIDATION AND VERIFICATION

In this section numerical results are presented. A set of simulations with at least 3 grids is carried out for each of the six Froude numbers. Grid uncertainty U_G and iterative uncertainty U_I are determined following Stern et al. (2001) [9]. Iterative uncertainty U_I is calculated as the largest amplitude of oscillatory converging signal in last few hundreds iterations (time steps):

$$U_I = \left|\frac{1}{2}\left(S_U - S_L\right)\right|, \quad (6)$$

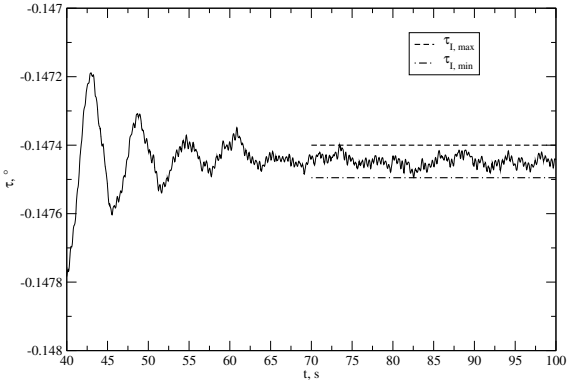

Figure 1: Example of iterative uncertainty determination for trim in $F_r = 0.282$ case on the finest grid.

where S_U and S_L stand for the maximum and minimum value of the oscillating result, as shown in Fig. 1. Determining the grid uncertainty U_G depends on the observed grid convergence type. In the case of monotone convergence grid uncertainty is calculated using the achieved order of spatial accuracy. Order of accuracy is determined using Richardson extrapolation:

$$p_G = \frac{\ln(\epsilon_{k_{32}}/\epsilon_{k_{21}})}{\ln(r_G)}, \quad (7)$$

where $\epsilon_{k_{32}} = S_3 - S_2$ is the difference between the result obtained with the coarsest grid (S_3) and the medium grid (S_2), and $\epsilon_{k_{21}} = S_2 - S_1$, where S_1 is the finest grid solution. r_G is the average grid refinement ratio. Grid uncertainty for monotone convergence is finally obtained as:

$$U_G = \frac{\epsilon_{k_{21}}}{r_G^{p_G} - 1}. \quad (8)$$

In the case of oscillatory grid convergence, U_G is determined as:

$$U_G = \left|\frac{1}{2}\left(S_{GU} - S_{GL}\right)\right|, \quad (9)$$

where S_{GU} stands for the maximum result among the grid solutions, and S_{GL} the minimum result. In the case of non–converging behaviour, U_G is calculated following Simonsen et al. [8] as:

$$U_G = \left|S_{GU} - S_{GL}\right|. \quad (10)$$

Simulation numerical uncertainty is calculated as:

$$U_{SN} = \sqrt{U_I^2 + U_G^2}. \quad (11)$$

Finally, following guidelines at the Workshop's website [6], total validation uncertainty can be calculated

using the experimental data uncertainty U_D and numerical simulation uncertainty U_{SN} as:

$$U_V = \sqrt{U_D^2 + U_{SN}^2}, \tag{12}$$

presenting overall estimate of the uncertainty which includes simulation and experimental uncertainties.

5.1 Simulation set–up

This section presents the summary of the CFD simulation set–up, while details concerning the model and experimental set–up can be found on the Workshop's website [6]. Domain spans 4.5 ship lengths in the longitudinal direction and 11 ship breadths in the transversal direction. Only half of the ship is simulated using symmetry boundary condition. Forward speed of the ship is modelled using constant current, thus the ship does not move in the longitudinal direction. Wave relaxation zone [3] is placed in the outlet region of the domain, where calm water surface is enforced to prevent possible wave reflection. Maximum Courant–Friedrichs–Lewy (CFL) number ranges from 10 to 50, allowing large time steps. Lower Froude number cases demanded lower CFL numbers to ensure convergence. Four grids that are used have approximately 600 000, 950 000, 2 600 000 and 4 600 000 cells. As constant grid refinement ratio is nearly impossible to achieve for unstructured grids, an average refinement ratio of $r_G = 1.28$ is used in uncertainty estimate for monotone grid convergence. Maximum grid non–orthogonality is approximately 80^o, while the maximum aspect ratio is 760. Grids are composed mostly of hexahedral cells further away from the hull, with prismatic and polyhedral cells used to form the boundary layer refinement.
The simulations are performed with Intel Core i5-3570K CPU processor at 3.40GHz on a desktop computer using 4 cores. As an example, for the highest Froude number $F_r = 0.282$ on the finest grid, convergence is reached after 2 380 time–steps, which took 70 hours of CPU time. For the second finest grid it took 3 950 time–steps in 58 hours of CPU time. The 600 000 and 950 000 cells grids took $\approx$ 1 800 time-steps to converge, requiring 6.5 and 10 hours of CPU time, respectively.

5.2 Total resistance

Fig. 2 shows result comparison for total resistance coefficient C_t. Uncertainty intervals are also presented with horizontal bars, where EFD stands for Experimental Fluid Dynamics (experimental data), while CFD denotes present simulation results. It can be seen that uncertainty generally reduces for larger Froude numbers. Such trend is expected as the boundary layer and free surface resolution of the grids is optimal for the design Froude number, thus making the grids unsuitable for lower Froude numbers.
Table 1 shows validation data for the total resistance. ϵ_{C_T} stands for the relative error, while E_{C_T} is the absolute error. Grid number 4 denotes the coarsest grid, while number 1 denotes the finest grid. Relative errors on the finest grids are smaller than 2%, except for the two smallest Froude number cases where the error remains within 5%. Relative error obtained with the finest grid for the deisgn Froude number is 0.4%. The errors are generally reducing for higher Froude numbers, which is expected, considering boundary layer and free surface resolution with respect to the flow field.
Verification results are shown in Table 2, where S_1 stands for the finest grid solution. For three cases the grid uncertainty is smaller than 3%. For Froude numbers $F_r = 0.108$ and 0.195 total resistance does not converge with grid refinement and uncertainty is calculated as the largest difference between the solutions, following Simonsen et al. [8]. Grid uncertainties remain lower than 6% for all cases, except for the design Froude number $F_r = 0.260$. High uncertainty in this case is caused by the low order of accuracy p_G, since monotone convergence has been achieved. The rate of change of the relative error for the three grids is close to linear, causing the low order of accuracy. Reason for this could be that the converged solution is not in the asymptotic range [5], as well as the use of unstructured, non–systematically refined grids. Iterative uncertainty U_I is expectedly small for all cases, except in the case of $F_r = 0.227$, where the larger value is caused by the very small normalisation value $\epsilon_{k_{21}}$.

5.3 Dynamic sinkage

Comparison of dynamic sinkage σ for a range of Froude numbers is shown in Fig. 3. Positive sinkage denotes upward displacement of the centre of gravity. It can be seen that the trend of change of sinkage for different Froude numbers is well described. Individual values also compare well with experimental results, as also can bee seen in Table 3. It can be seen that the error is consistently reducing for higher Froude numbers. For the three largest Froude numbers relative errors obtained with the finest grid are smaller than 4%. Relative error for the $F_r = 0.195$ case is $\approx$ 15%, and it further increases for smaller Froude numbers. The smallest Froude number case has a relative error

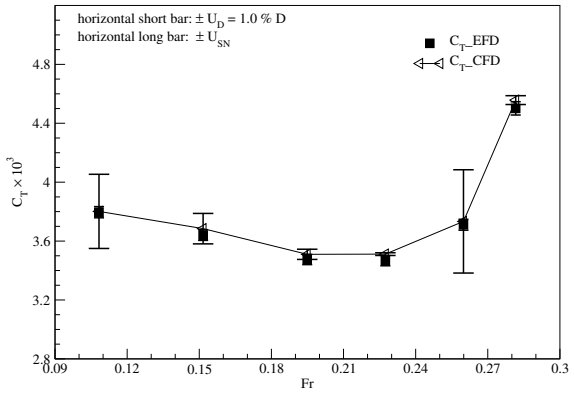

Figure 2: Comparison of total resistance coefficient with error bars.

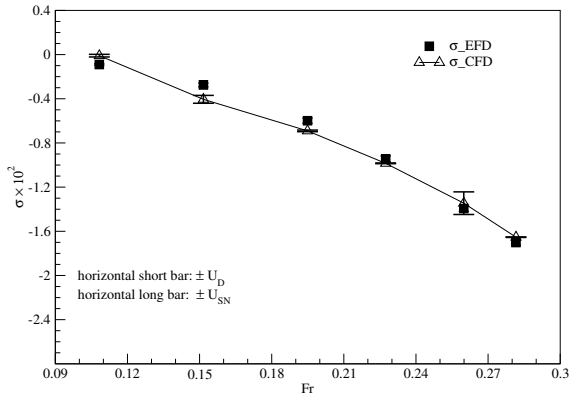

Figure 3: Dynamic sinkage comparison with error bars.

Table 1: C_t validation results.

F_r	Grid No.	$\epsilon_{C_t}, \%$	$E_{C_T} \cdot 10^3$
0.108	3	-11.8	-0.446
	2	-9.1	-0.345
	1	-4.6	-0.175
0.152	3	-9.1	-0.331
	2	-6.5	-0.237
	1	-4.9	-0.178
0.195	3	-7.0	-0.244
	2	-6.2	-0.216
	1	-1.5	-0.051
0.227	4	-5.9	-0.205
	3	-4.8	-0.168
	2	-2.1	-0.071
	1	-2.0	-0.069
0.260	4	-7.3	-0.270
	3	-5.4	-0.199
	2	-2.6	-0.097
	1	-0.4	-0.015
0.282	4	-7.5	-0.336
	3	-5.2	-0.236
	2	-2.4	-0.107
	1	-1.3	-0.059

Table 2: C_t verification results.

F_r	p_G	$U_I/\epsilon_{k_{21}}$	$U_G/S_1, \%$	U_V
0.108	N/A	$-9.36 \cdot 10^{-3}$	6.8	0.2734
0.152	1.85	$-5.82 \cdot 10^{-2}$	2.7	0.1096
0.195	N/A	$-5.18 \cdot 10^{-2}$	5.5	0.1964
0.227	16.0	-5.09	0.0	0.0359
0.256	0.86	$-3.15 \cdot 10^{-1}$	9.4	0.3528
0.282	3.98	$-1.79 \cdot 10^{-1}$	0.6	0.0541

of approximately 100%, however the absolute magnitude of the error is very small, and we do not expect to resolve such a small sinkage with relatively coarse grid. Absolute error is ≈ 0.1mm, while the cell height at the free surface is ≈ 0.5mm. Dynamic sinkage is largely influenced by the wave pattern generated by the ship. For lower Froude numbers, generated waves are smaller, and thus they are less accurately resolved since the same grids are used for all Froude numbers. This is most likely the main reason for the larger relative errors of sinkage for lower Froude numbers. This relation can also be used in the opposite direction, to state an assumption that the wave pattern is well predicted for higher Froude numbers.
Sinkage verification is outlined in Table 4. Grid uncertainty is often smaller than $\approx 1\%$. For the two lowest Froude numbers grid uncertainty is 3% to 4%. As for the total resistance coefficient, sinkage at the design Froude number exhibits the largest grid uncertainty. Again, this is caused by the low order of spatial accuracy as the monotone convergence is achieved. Iterative uncertainty is negligibly small in all cases.

5.4 Dynamic trim

Fig. 4 shows the comparison of dynamic trim τ for a range of Froude numbers. Positive trim is defined for bow up motion. As shown in Fig. 4, rate of change of trim over different Froude number values is well captured by CFD simulations. Table 5 shows validation results for trim. In most cases the relative error is smaller than 10%, while the relative error for the design Froude number is 1%. In most cases the error is not changing significantly with respect to grid refinement. For example, absolute error for the highest Froude number changes only 0.0002 degrees from

Table 3: Sinkage validation results.

F_r	Grid No.	$\epsilon_\sigma, \%$	E_σ, cm
0.108	3	-122.1	-0.110
	2	-115.6	-0.104
	1	-109.0	-0.098
0.152	3	-53.7	-0.148
	2	-50.4	-0.139
	1	-40.4	-0.112
0.195	3	-18.4	-0.110
	2	-16.4	-0.098
	1	-15.3	-0.092
0.227	4	-6.8	-0.064
	3	-4.7	-0.044
	2	-4.6	-0.043
	1	-4.3	-0.041
0.260	4	1.3	-0.017
	3	3.0	-0.042
	2	3.3	-0.045
	1	3.5	-0.049
0.282	4	2.2	-0.037
	3	3.1	-0.052
	2	2.8	-0.047
	1	2.9	-0.049

Table 4: Sinkage verification results.

F_r	p_G	$U_I/\epsilon_{k_{21}}$	$U_G/S_1, \%$	U_V
0.108	N/A	$1.98{\cdot}10^{-5}$	6.3	0.0139
0.152	N/A	$1.05{\cdot}10^{-5}$	9.2	0.0392
0.195	2.57	$3.29{\cdot}10^{-5}$	1.1	0.0245
0.227	3.7	$7.64{\cdot}10^{-4}$	0.4	0.0265
0.256	0.13	$4.00{\cdot}10^{-3}$	7.6	0.1056
0.282	N/A	$2.59{\cdot}10^{-4}$	0.2	0.0233

the smallest to the largest error. The smallest Froude number case suffers larger relative errors due to the extremely small trim measured in experiments, which is comparable to the magnitude of absolute errors in most cases. Thus, the relative error is not a good measure for assessing the accuracy in this case. It can be concluded from this observation that all grids used in this study are too coarse for more accurate trim calculation at very low Froude numbers. For example, the largest trim causes only 1mm of vertical displacement at the front and aft perpendicular of the ship. Unlike the resistance and sinkage results, trim results do not show the consistent deterioration for lower Froude numbers.

Table 6 shows the verification data for trim. Grid uncertainty is fairly small for most cases, not exceeding 1.2% for the largest three Froude number cases.

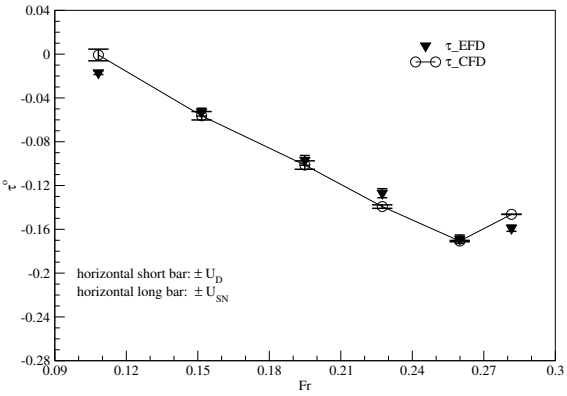

Figure 4: Comparison of dynamic trim with error bars.

The three smaller Froude number cases show larger uncertainty, which is expected. Only the largest Froude number case exhibits monotonic convergence, while the rest show oscillatory convergence or non–converging behaviour. For all Froude numbers, iterative uncertainty is negligibly small compared to grid uncertainty.

Table 5: Trim validation results.

F_r	Grid No.	$\epsilon_\tau, \%$	$E_\tau, ^o$
0.108	3	-106.1	0.018
	2	-97.2	0.017
	1	-74.8	0.013
0.152	3	-14.7	0.008
	2	-12.0	0.006
	1	-7.5	0.004
0.195	3	-10.7	0.010
	2	-2.8	0.003
	1	-5.1	0.005
0.227	4	-14.6	0.019
	3	-8.3	0.011
	2	-10.8	0.014
	1	-9.6	0.012
0.260	4	-3.2	0.005
	3	-0.9	0.001
	2	-0.3	0.000
	1	-1.0	0.002
0.282	4	8.8	-0.014
	3	7.3	-0.012
	2	7.9	-0.012
	1	8.0	-0.013

Table 6: Trim verification results.

F_r	p_G	$U_I/\epsilon_{k_{21}}$	$U_G/S_1, \%$	U_V
0.108	N/A	$4.62{\cdot}10^{-6}$	17.9	0.003
0.152	N/A	$1.05{\cdot}10^{-5}$	6.7	0.005
0.195	N/A	$-1.69{\cdot}10^{-4}$	3.8	0.006
0.227	N/A	$-5.04{\cdot}10^{-4}$	1.2	0.004
0.256	N/A	$-7.65{\cdot}10^{-3}$	0.4	0.0039
0.282	6.21	$2.57{\cdot}10^{-3}$	0.04	0.0028

6 CONCLUSION

A detailed numerical study concerning steady resistance of the KCS model with dynamic sinkage and trim is performed. Simulation are performed for six Froude numbers on at least three grid (for each Froude number). Grid convergence study is performed to determine uncertainties of the numerical simulations. The embedded free surface approach inside the `Naval Hydro` pack is used.

For steady resistance, monotone grid convergence is achieved for four cases, while two cases did not converge with grid refinement. Average grid uncertainty is 3.5%. The resistance is well predicted, average relative error being less than 2.5% on the finest grids, and only 0.4% for the design Froude number.

Sinkage shows overall good agreement with experimental data, with only 3.5% average error for the three higher Froude numbers. Lower Froude numbers suffer larger relative errors, mainly due to insufficient grid resolution for small motions. Monotone grid convergence is achieved for half of the cases, one case exhibited oscillatory convergence, and for the two lowest Froude number cases non–convergent behaviour occurred with grid refinement. However, average grid uncertainty is 2.6%.

Taking into account relative grid resolution in respect to trim magnitudes, results show good agreement with experimental data. Average relative error obtained on the finest grid is $\approx 6.2\%$, excluding the lowest Froude number case. Average grid uncertainty is $\approx 3.4\%$, however monotone convergence is seldom achieved. Three cases exhibited oscillatory convergence, and the two lowest Froude number cases did not achieve grid convergence. Grid convergence difficulties are probably caused by the narrow–boundedness of trim results, where a small perturbation causes oscillatory convergence or lack of convergence.

Overall, the measured items are well predicted with CFD for a range of Froude numbers, yielding small errors and numerical uncertainties. For a more accurate study from the trim and sinkage point of view, finer grids should be used.

References

[1] I. Demiridžić and M Perić. Space conservation law in finite volume calculations of fluid flow. *Int. J. Numer. Meth. Fluids*, 8:1037–1050, 1998.

[2] J. Huang, P. M. Carrica, and F. Stern. Coupled ghost fluid/two–phase level set method for curvilinear body–fitted grids. *Int. J. Numer. Meth. Fluids*, 44:867–897, 2007.

[3] N. G. Jacobsen, D. R. Fuhrman, and J. Fredsøe. A wave generation toolbox for the open-source CFD library: OpenFoam®. *Int. J. Numer. Meth. Fluids*, 70(9):1073–1088, 2012.

[4] H. Jasak. *Error Analysis and Estimation for the Finite Volume Method with Applications to Fluid Flows*. PhD thesis, Imperial College of Science, Technology & Medicine, London, 1996.

[5] L. Larsson, F. Stern, and M. Vissoneau. *Numerical Ship Hydrodynamics: An assessment of the Gothenburg 2010 workshop*. Springer, 2013.

[6] National Maritime Reasearch Inistitute (NMRI). Tokyo 2015: A Workshop on CFD in Ship Hydrodynamics. `http://www.t2015.nmri.go.jp/`, 2015. [Online; accessed 20 August 2015].

[7] H. Rusche. *Computational Fluid Dynamics of Dispersed Two - Phase Flows at High Phase Fractions*. PhD thesis, Imperial College of Science, Technology & Medicine, London, 2002.

[8] C. D. Simonsen, J. F. Otzen, S. Joncquey, and F. Stern. EFD and CFD for KCS heaving and pitching in regular head waves. *J. Mar. Sci. Technol.*, 18:435–459, 2013.

[9] F. Stern, R. V. Wilson, H. W. Coleman, and E. G. Paterson. Comprehensive Approach to Verification and Validation of CFD Simulations–Part 1: Methodology and Procedures. *J. Fluids. Eng*, 123(4):793–802, 2001.

[10] V. Vukčević and H. Jasak. Embedded Free Surface Method in Polyhedral Finite Volume Framework: Part I: Computational Method. *Submitted to Journal of Computational Physics*, ??:???–???, 2015.

[11] D. C. Wilcox. *Turbulence Modeling for CFD*. DCW Industries, 1993.